

Relationship of box counting of fractured rock mass with Hoek-Brown parameters using particle flow simulation

Jianguo Ning, Xuesheng Liu^{*}, Yunliang Tan, Jun Wang and Chenglin Tian

State Key Laboratory of Mining Disaster Prevention and Control Co-founded by Shandong Province and the Ministry of Science and Technology, Shandong University of Science and Technology, 266590 Qingdao, China

(Received December 18, 2014, Revised June 02, 2015, Accepted June 05, 2015)

Abstract. Influenced by various mining activities, fractures in rock masses have different densities, set numbers and lengths, which induce different mechanical properties and failure modes of rock masses. Therefore, precisely expressing the failure criterion of the fractured rock influenced by coal mining is significant for the support design, safety assessment and disaster prevention of underground mining engineering subjected to multiple mining activities. By adopting PFC2D particle flow simulation software, this study investigated the propagation and fractal evolution laws of the micro cracks occurring in two typical kinds of rocks under uniaxial compressive condition. Furthermore, it calculated compressive strengths of the rocks with different confining pressures and box-counting dimensions. Moreover, the quantitative relation between the box-counting dimension of the rocks and the empirical parameters m and s in Hoek-Brown strength criterion was established. Results showed that with the increase of the strain, the box-counting dimension of the rocks first increased slowly at the beginning and then exhibited an exponential increase approximately. In the case of small strains of same value, the box-counting dimensions of hard rocks were smaller than those of weak rocks, while the former increased rapidly and were larger than the latter under large strain. The results also presented that there was a negative correlation between the parameters m and s in Hoek-Brown strength criterion and the box-counting dimension of the rocks suffering from variable mining activities. In other words, as the box-counting dimensions increased, the parameters m and s decreased linearly, and their relationship could be described using first order polynomial function.

Keywords: fractured rock mass; Hoek-Brown strength criterion; rock mass parameters; box-counting dimension; numerical simulation

1. Introduction

Since proposed in 1980, Hoek-Brown strength criterion has drawn extensive attention in academic circles and engineering fields (Bagheripour *et al.* 2011, Nekouei and Ahangari 2013, Monkul 2013, Yang and Pan 2015, Yang and Qin 2014, Shen *et al.* 2013). It is an empirical strength criterion on the basis of rock mechanics tests. There are two important empirical parameters, m and s , in the criterion, which are related to the characteristics and fragmentation degree of rock mass. Acquiring rock mass parameters m and s explicitly is essential for the accurate judgment of rock mass failures (Hoek *et al.* 2002, Bejarbaneh *et al.* 2015, Yang *et al.*

^{*}Corresponding author, Ph.D., E-mail: xuesheng1134@163.com

2013, Langford and Diederichs 2015, Ismael 2014, Senent *et al.* 2013). Hoek *et al.* introduced the lookup table estimation, statistics of indoor triaxial test, estimating based on RMR index, statistics of *in situ* direct shear or large-sized shear experiments (1998), and estimating by geomechanics index GSI and disturbance parameter D (2002) successively. Numerous fruitful research have been done by Song and Yu (2001), Palmstrom (1996), and Zhang *et al.* (2000) on the method for obtaining values of parameters m and s , which has promoted the engineering application of Hoek-Brown strength criterion.

For most of the underground mining projects, such as the mining of coal seam group in close distance, the overlying strata encounter several mining activities. The mechanical properties and failure modes vary significantly owing to different densities, set numbers and lengths of fractures in rock masses affected by different mining activities. Existing methods for obtaining values of rock mass parameters m and s in Hoek-Brown strength criterion fail to describe the mechanical behaviors and failure criterion of rocks which are fractured in different mining activities. In fact, the parameter m in Hoek-Brown strength criterion is a macro mechanical parameter for reflecting the characteristics of rock mass, and the greater the mining influences, the smaller the parameter is. While parameter s mirrors the fragmentation degree of rocks; and the higher the degree is, the smaller the parameter is. These phenomena demonstrate that for those rock masses influenced by different mining activities, the values of the parameters m and s are closely related to the distributions, scales, etc. of cracks inside the rocks. Many researchers studied the evolutions of acoustic emissions during the progressive cracking of rocks and tried to use acoustic emission activities to describe the cracking degree of rocks (Aker *et al.* 2014, Amitrano *et al.* 2012, Cheon *et al.* 2011). However, it is an indirect method and cannot be directly used in any strength criterions. Previous research interprets that the distribution, structure, and evolution of the internal fractures of rock materials with load show obvious statistical self-similarities in the form of fractals which can be described using the box-counting (Vallejo 2012, Ai *et al.* 2014, Li and Huang 2015, Yuan and Li 2009). Therefore, it is effective to determine the criterion of fractured rock mass using Hoek-Brown strength criterion by constructing the relationship between box-counting dimension of rock mass and the parameters m and s . The method is important for the support design, safety evaluation and disaster prevention of underground mining engineering subjected to multiple mining activities.

Two typical rock specimens including hard siltstone and soft sandy mudstone were selected and PFC2D particle flow simulation software was adopted to acquire the micro parameters corresponding to the macro mechanical properties of the two kinds of rock specimens. Then, this paper studied the propagation and fractal evolution laws of the rock micro cracks under the uniaxial compressive condition and calculated the compressive strengths of the rocks under different confining pressures and box-counting dimensions. Finally, the quantitative relation between the box-counting dimension of the rocks and the parameters m and s in Hoek-Brown strength criterion was established.

2. Typical rock specimens and their macro mechanical parameters

Type 1 rock specimens were obtained from the main roof of 8704 coal face in No. 11 coal seam (Xinzhouyao Mine of Datong Coal Mining Group Company, Shanxi Province, China). Type 2 rock specimens were acquired from the main roof of 20307 coal face in No. 2^{upper} coal seam (Haohua Clean Coal Mine Co. Ltd, Ordos City, Inner Mongolia, China). The type 1 rock

specimens are Jurassic siltstones which are compact, cemented, hard, and likely to be brittle damaged. While type 2 samples are Jurassic sandy mudstones with pelitic structure, poor cementation, low strength and easily to be softened when encounter water.

According to the regulations in the *Standard for Tests method of Engineering Rock Masses* (GB/T 50266-2013), the MTS815 electro-hydraulic servo rock mechanical test system was employed to apply uniaxial loads on the aforementioned rock specimens. The specimens were processed to be standard cylinders which were 50 mm in diameter and 100 mm in height, and tested at the loading speed of 0.05 mm/min. The physical and mechanical properties of the rock specimens obtained are displayed in Table 1 and the stress-strain curve and the failure characteristics at each stage are revealed in Fig. 1.

Fig. 1 shows that there are few micro cracks and no macro fissure on the type 1 specimens when the stress loaded is smaller than the peak strength. While, the amount of micro cracks

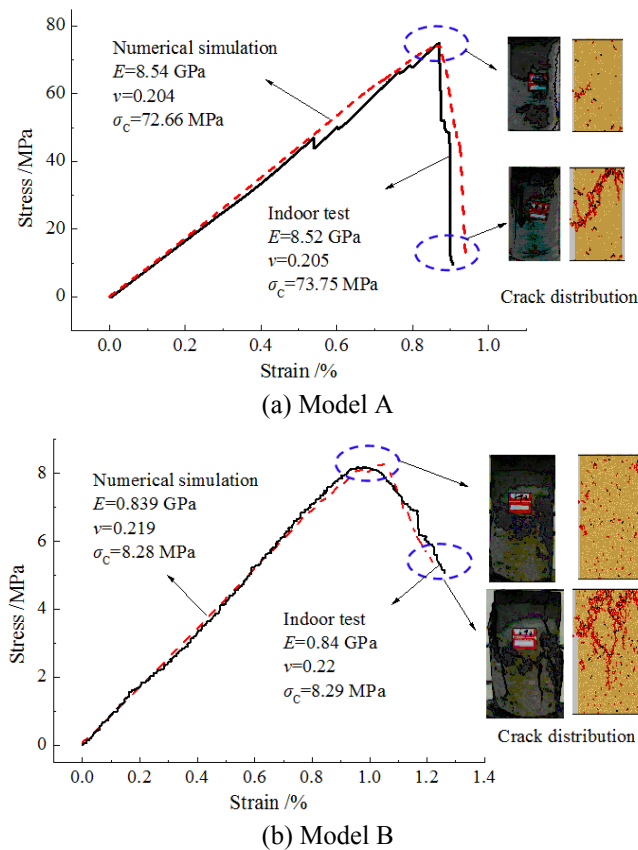


Fig. 1 Comparison between numerical simulation and indoor test: (a) Model A; (b) Model B

Table 1 The physical and mechanical properties of the rock specimens

Specimens	Density/g·cm ⁻³	Young's modulus /GPa	Poisson's ratio	Uniaxial compressive strength/MPa
Type 1	2.66	8.52	0.205	72.75
Type 2	2.32	0.84	0.22	8.47

increases dramatically when the stress exceeds the peak one, and then the specimens are suddenly damaged. Compared with type 1 specimens, the type 2 specimens show more micro cracks with one or two macro fissures when the stress reaches to the peak value. In the case of exceeding the peak strength, the specimens are destroyed gradually with small rupture blocks.

3. Propagation of micro cracks and fractal evolution laws under uniaxial compressive condition

3.1 Model building and determination of the micro parameters

Model building

Numerical simulation is performed utilizing PFC2D software for the rectangle specimens which are 50 mm in width and 100 mm in height and enclosed in a frame with upper, lower, left and right walls. In order to avoid the overflow of the particles, the size of walls is 1.2 times larger than that of the specimens. Rigid circular particles are used as the specimen subject, and they are uniformly distributed in size. According to literature (Jensen *et al.* 1999, Wang *et al.* 2014), the reasonable ratio between the specimen sizes and the average particle size d_{50} of internal particles should be larger than 30~40. The minimum particle size R_{\min} is set as 0.4 mm and the ratio between the maximum and minimum particle sizes R_{\max}/R_{\min} is 2.0 in the simulation. The contacts among particles are simulated using parallel bond, which can transmit force and torque and simulate compact materials such as coal rock. The parameters of parallel bond include normal stiffness, shear stiffness, normal strength, shear strength, and bond radius. The loading rate of the model specimen is the same as that of indoor test which is also set as 0.05 mm/min.

Determination of the micro parameters

The main micro parameters have to be set in the model are contact parameters and bond parameters of the particles. Among which, the contact parameters comprise the Young's modulus E_c at each contact, the ratio k_n/k_s of particle normal to shear stiffness, and the friction coefficient μ among particles. While, the bond parameters include multiplier $\bar{\lambda}$ of bond radius, the Young's modulus \bar{E}_c of each parallel bond, the ratio \bar{k}_n/\bar{k}_s of parallel bond normal to shear stiffness, the average normal strength $\bar{\sigma}_c$ and shear strength $\bar{\tau}_c$ of the bond.

The normal stiffness k_n and the shear stiffness k_s of the particle contact and the normal stiffness \bar{k}_n and the shear stiffness \bar{k}_s of the bond can be expressed as (Potyondy and Cundall 2004)

$$\begin{cases} k_n = 2tE_c, & t = 1 \\ k_s = \frac{k_n}{k_n/k_s} \end{cases} \quad \begin{cases} \bar{k}_n = \frac{\bar{E}_c}{R^{(1)} + R^{(2)}} \\ \bar{k}_s = \frac{\bar{k}_n}{\bar{k}_n/\bar{k}_s} \end{cases} \quad (1)$$

where $R^{(1)}$ and $R^{(2)}$ represent the radii of two contacted particles.

Through biaxial compression test and repeated adjustments for test parameters, two groups of micro parameters A and B (see Table 2) are obtained. The macro mechanical characteristics involving Young's modulus, Poisson's ratios, tensile and compressive strengths, and failure modes,

Table 2 Micro parameters of PFC2D models

Models	$\rho / \text{g}\cdot\text{cm}^{-3}$	R_{\min} / mm	R_{\max}/R_{\min}	E_c / GPa	k_n/k_s	M
Model A	2.63	0.4	2.0	6.4	2.1	0.5
Model B	2.43	0.4	2.0	0.9	2.4	0.4
Models	$\bar{\lambda}$	\bar{E}_c / GPa	\bar{k}_n / \bar{k}_s	$\bar{\sigma}_c / \text{MPa}$	$\bar{\tau}_c / \text{MPa}$	
Model A	1.0	6.8	2.0	57.5	49	
Model B	1.2	0.4	2.0	5.2	5.0	

in PFC2D particle flow models A (simulating the type 1 rock specimens adopting micro parameters in group A) and B (simulating the type 2 rock specimens employing the micro parameters in group B) are identical to the indoor test results of the two kinds of rock specimens. The stress-strain curve is shown in Fig. 1.

3.2 Simulation results

The uniaxial loading tests of different grades were conducted for the type 1 specimens (model A) and the type 2 specimens (model B). In each test, the specimens were unloaded at the stress of 60%, 70%, 80%, 90%, and 100% of the peak strength and 90%, 80%, and 60% of the peak after exceeding the peak, respectively. Distributions of the micro cracks inside the rocks under different loadings are displayed in Figs. 2 and 3. Fig. 2(a) illustrates that in the case of small loadings, the

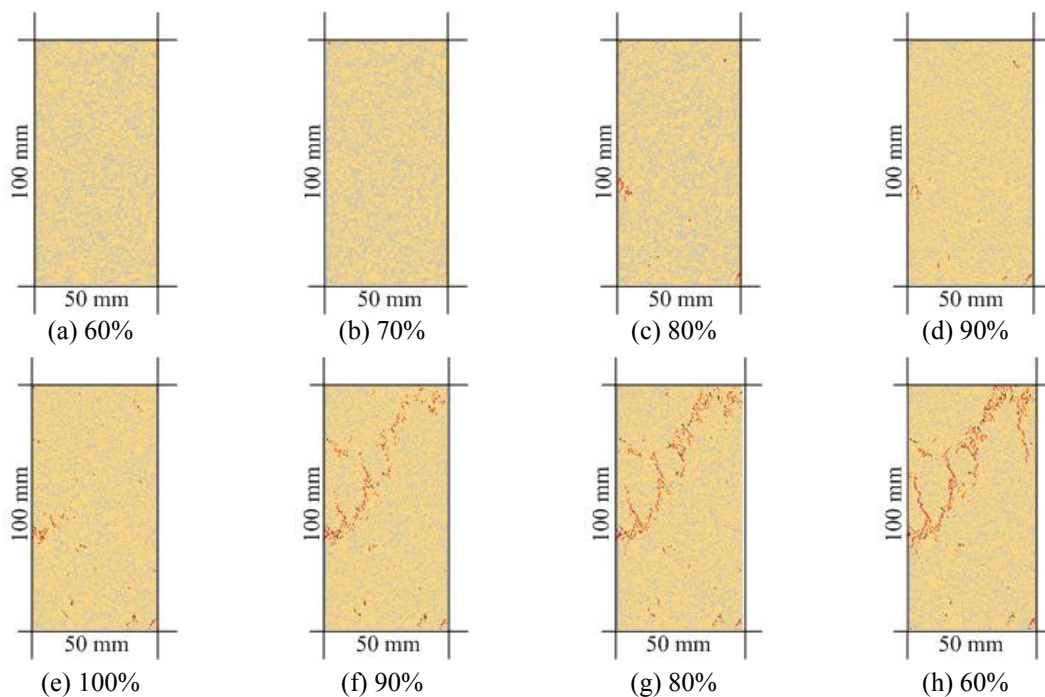


Fig. 2 Crack distribution of Model A unloaded at different stress: (a)~(e) are at pre-peak phase; (f)~(h) are at post-peak phase

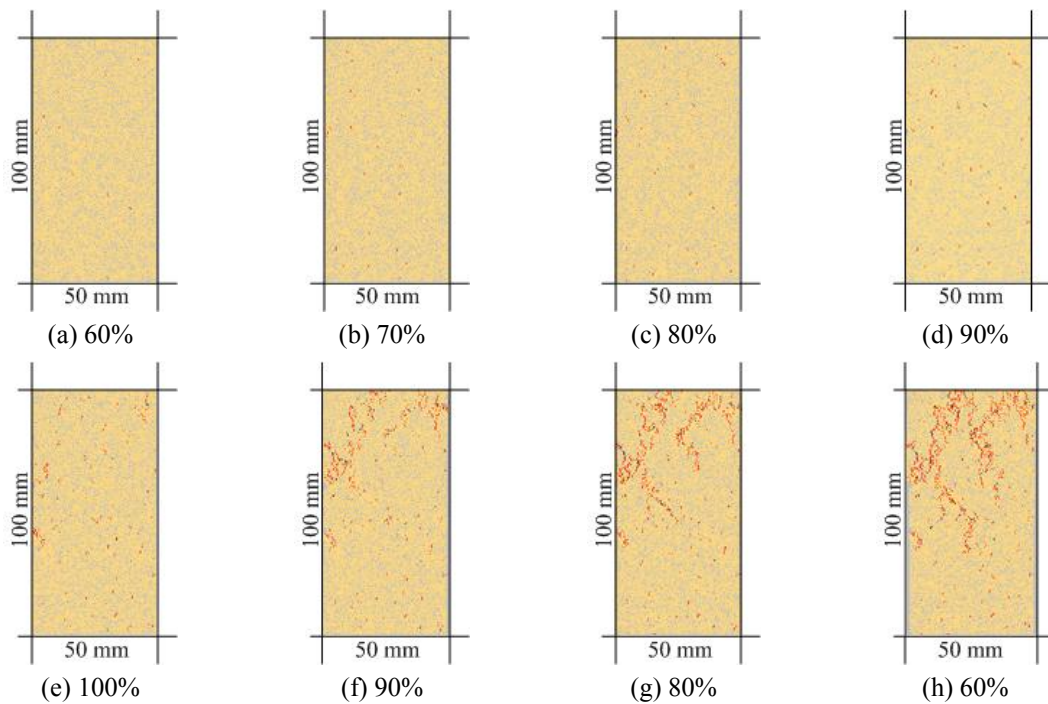


Fig. 3 Crack distribution of Model B unloaded at different percent of peak strength: (a)~(e) are at pre-peak phase; (f)~(h) are at post-peak phase

particles inside the rock present good cementation without micro cracks. When 70% and 60% of the peak strength are loaded on the types 1 and 2 specimens, respectively, the micro cracks are found in the rocks. When the load is increased, the amount of micro cracks raises gradually; while after exceeding the peak strength, the micro cracks increase, propagate, and run-through each other rapidly, thus forming macro fractures.

In order to quantitatively describe the propagation law of micro cracks in the rocks, the fractal geometry theory was introduced. The fractal dimension was used to quantitatively describe the distribution and evolution of the micro cracks inside the rocks. Owing to the complexity of direct calculation for Hausdorff dimension, this study employed the box-counting dimension to depict the fractal evolution law of the micro cracks in the rocks.

The FRACLAB toolbox of MATLAB software was utilized to calculate the box-counting dimension. Firstly, by applying the `im2bw` function, binaryzation was performed for the distributions (as displayed in Figs. 2 and 3) of the micro cracks in the rocks, and the pixel information was preserved in the matrix. Afterwards, the FRACLAB toolbox was imported in to calculate the box-counting dimension after adjusting the size of the box. Line segment with stable slope was selected from the calculation results, the slope of which was the box-counting dimension of the image. Table 3 exhibits the calculation results of the box-counting dimensions of the micro crack distributions in Figs. 2 and 3; Fig. 4 shows the relationship between the box-counting dimension and the strain.

It is observed from Fig. 4 that as the strain increases, the box-counting dimension first increases slowly, and then increases exponentially after exceeding certain strain (for the types 1 and 2 rock

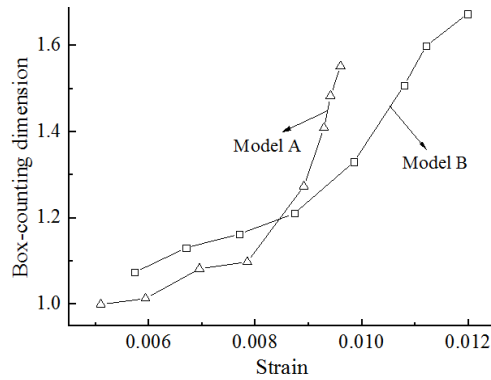


Fig. 4 Relationship between the box-counting dimension and the strain

Table 3 Box-counting dimension of specimens with different loading

Models	Box-counting dimension							
	a	b	c	d	e	f	g	h
Model A	1.0000	1.0135	1.0823	1.0984	1.2735	1.4092	1.4833	1.5518
Model B	1.0739	1.1310	1.1628	1.2107	1.3305	1.5074	1.5996	1.6729

*Notes: (a)~(h) in the table are the corresponding models of (a)~(h) in Figs. 2 and 3, respectively

specimens, the strains are about 0.008 and 0.009, respectively). When the strain is less than 0.0084, the box-counting dimension of the type 1 specimens is smaller than that of the type 2 under the same strain. In the case that the strain exceeds 0.0084, the box-counting dimension of the type 1 specimens is larger than that of the type 2 under the same strain.

4. Relationship between the box-counting dimension and the parameters m and s

4.1 Variations of compressive strength

Triaxial compression test was carried out for the aforementioned rock models with different box-counting dimensions. The confining pressures loaded on each rock model were about 15%, 25%, 40%, 50% and 60% of the uniaxial compressive strength. For the type 1 specimens (model A), the confining pressures were 10.9, 18.2, 29.1, 36.3 and 43.6 MPa, respectively. While for the type 2 specimens, the confining pressures were 1.2, 2.1, 3.3, 4.1 and 5.0 MPa, respectively. By collecting the compressive strengths of various rocks under different confining pressures, the variation curve of compressive strengths with confining pressures and the box-counting dimensions was obtained and displayed in Fig. 5.

The figure shows that all the compressive strengths of the rocks with different box-counting dimensions rise with the increase of the confining pressure. For the type 1 rock specimens with different box-counting dimensions, when the confining pressure rises from 10.9 to 43.6 MPa, the maximum and minimum compressive strengths of the rock specimens increase by 69.7% and 119.3%, respectively. For the type 2 rock specimens with various box-counting dimensions, in the case that the confining pressure increases from 1.2 to 5.0 MPa, the maximum and minimum

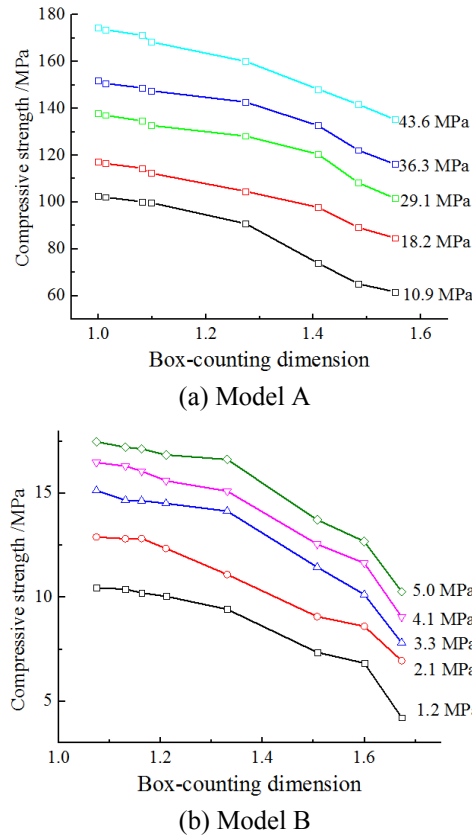


Fig. 5 Variations of compressive strengths with confining pressures and the box-counting dimensions

compressive strengths of the rocks increase by 39.9% and 22.4%, respectively. Under the same confining pressure, the compressive strength of the rocks decreases linearly as the box-counting dimension increases. For the type 1 rock specimens, when the box-counting dimension increases from 1.0 to 1.5518, the maximum and minimum compressive strengths of the rocks decrease by 39.9% and 22.4%, respectively. While for the type 2 rock specimens, as the box-counting dimension rises from 1.0739 to 1.6729, the maximum and minimum compressive strengths of the rocks decrease by 41.2% and 59.8%, respectively.

4.2 Calculating of parameters m and s

The method for determining the rock parameters m and s by performing laboratory triaxial compression test was put forward by Hoek and Brown in 1980. Parameters m and s were separately confirmed using the following equations

$$m = \frac{1}{\sigma_c} \left[\frac{\sum x_i y_i - \frac{\sum x_i \sum y_i}{n}}{\sum x_i^2 - \frac{(\sum x_i)^2}{n}} \right] \quad (2)$$

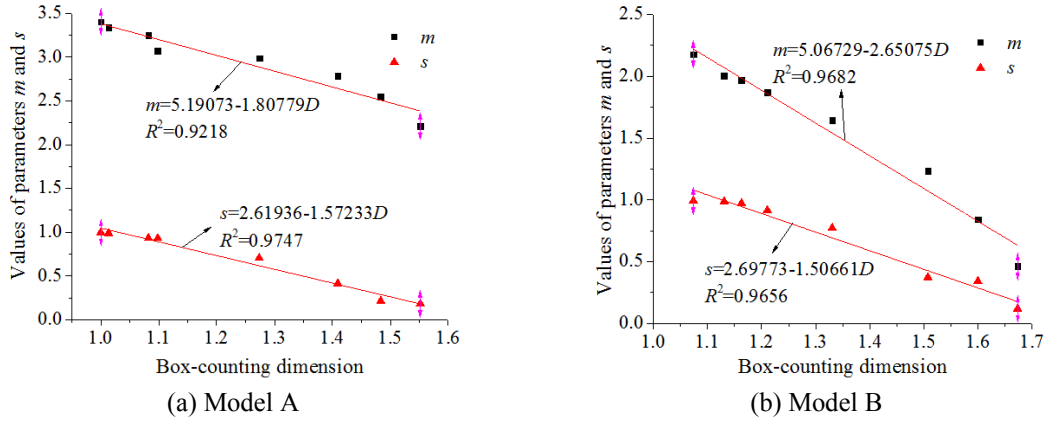


Fig. 6 Values of parameters m and s of models with different box-counting dimension and their fitting curves

$$s = \frac{\frac{1}{n} \sum y_i - \frac{1}{n} m \sigma_C \sum x_i}{\sigma_C^2} \tag{3}$$

in which

$$x = \sigma_3, \quad y = (\sigma_1 - \sigma_3)^2 \tag{4}$$

where n is the number of data group of σ_1 and σ_3 , usually bigger than 5; σ_C is the uniaxial compressive strength of correspondingly intact rock.

By substituting the simulation results in Fig. 5 into Eqs. (2) and (3), the corresponding values of parameters m and s are acquired for the same rock with different box-counting dimensions. The variations of parameters m and s with the box-counting dimension are shown in Fig. 6, which demonstrates that both the rock parameters m and s decrease gradually with the increase of the box-counting dimension. The variation law can be favorably fitted by using first order polynomial function, that is, Eq. (5).

$$\begin{cases} m = a_1 + b_1 D \\ s = a_2 + b_2 D \end{cases} \tag{5}$$

where D is the box-counting dimension of models; a_1, a_2, b_1 and b_2 are the fitting parameters that are related to the physical and mechanical properties.

5. Conclusions

- (i) For both hard siltstone and soft sandy mudstone, the evolution laws of the internal micro cracks are highly correlated with their box-counting dimensions. With the increase of the strain, the box-counting dimension first increases slowly and then rises exponentially when the strain exceeds certain value.
- (ii) With the increase of the confining pressure, compressive strengths of the same rock with different box-counting dimensions increase correspondingly. Under the same confining

pressure, the compressive strengths of the same rock decrease linearly as the box-counting dimensions increase.

- (iii) The parameters m and s in Hoek-Brown strength criterion negatively correlated with the box-counting dimension of the same rock experiencing different mining activities. With the increase of the box-counting dimension, m and s decrease linearly, and the fit of the correlation using first order polynomial function exhibits high accuracy.
- (iv) The research is conducted only based on a particle flow simulation method and shows certain limitation. Results are expected to be verified and modified by carrying out numerous indoor experiments in the future.

Acknowledgments

This study was supported by National Natural Science Foundation of China (Nos. 51274133 and 51474137), Shandong Province Natural Science Fund (No. ZR2012EEZ002), Doctoral Scientific Fund Project of the Ministry of Education of China (No. 20123718110013) and Open Fund of State Key Laboratory of Mining Disaster Prevention and Control Co-founded by Shandong Province and the Ministry of Science and Technology (No. MDPC2013KF12).

References

- Ai, T., Zhang, R. and Zhou, H.W. (2014), "Box-counting methods to directly estimate the fractal dimension of a rock surface", *Appl. Surf. Sci.*, **314**, 610-621.
- Aker, E., Kühn, D., Vavryčuk, V., Soldal, M. and Oye, V. (2014), "Experimental investigation of acoustic emissions and their moment tensors in rock during failure", *Int. J. Rock Mech. Min. Sci.*, **70**, 286-295.
- Amitrano, D., Gruber, S. and Girard, L. (2012), "Evidence of frost-cracking inferred from acoustic emissions in a high-alpine rock-wall", *Earth Planet. Sc. Lett.*, **341-344**, 86-93.
- Bagheripour, M.H., Rahgozar, R., Pashnesaz, H. and Malekinejad, M. (2011), "A complement to Hoek-Brown failure criterion for strength prediction in anisotropic rock", *Geomech. Eng., Int. J.*, **3**(1), 61-81.
- Bejarbaneh, B.Y., Armaghani, D.J. and Amin, M.F.M. (2015), "Strength characterisation of shale using Mohr-Coulomb and Hoek-Brown criteria", *Measurement*, **63**, 269-281.
- Cheon, D.S., Jung, Y.B., Park, E.S., Song, W.K. and Jang, H.I. (2011), "Evaluation of damage level for rock slopes using acoustic emission technique with waveguides", *Eng. Geol.*, **121**, 75-88.
- Hoek, E. and Brown, E.T. (1980), "Empirical strength criterion for rock masses", *J. Geotech. Geoenviron. Eng.*, **106**(GT9), 1013-1035.
- Hoek, E., Marinos, P. and Benissi, M. (1998), "Applicability of the Geological Strength Index (GSI) classification for very weak and sheared rock masses: The case of the Athens Schist Formation", *B. Eng. Geol. Environ.*, **57**(2), 151-160.
- Hoek, E., Carranza-Torres, C. and Corkum, B. (2002), "Hoek-Brown failure criterion-2002 edition", *Proceedings of NARMS-Tac*, 267-273.
- Ismael, M.A., Imam, H.F. and El-Shayeb, Y. (2014), "A simplified approach to directly consider intact rock anisotropy in Hoek-Brown failure criterion", *J. Rock Mech. Geotech. Eng.*, **6**(5), 486-492.
- Jensen, R.P., Bosscher, P.J., Plesha, M.E. and Edil, T.B. (1999), "DEM simulation of granular media — structure interface: Effects of surface roughness and particle shape", *Int. J. Numer. Anal. Met.*, **23**(6), 531-547.
- Langford, J.C. and Diederichs, M.S. (2015), "Quantifying uncertainty in Hoek-Brown intact strength envelopes", *Int. J. Rock Mech. Min. Sci.*, **74**, 91-102.

- Li, Y.R. and Huang, R.Q. (2015), "Relationship between joint roughness coefficient and fractal dimension of rock fracture surfaces", *Int. J. Rock Mech. Min. Sci.*, **75**, 15-22.
- Monkul, M.M. (2013), "Influence of gradation on shear strength and volume change behavior of silty sands", *Geomech. Eng., Int. J.*, **5**(5), 401-417.
- Nekouei, A.M. and Ahangari, K. (2013), "Validation of Hoek–Brown failure criterion charts for rock slopes", *Int. J. Min. Sci. Technol.*, **23**(6), 805-808.
- Palmstrom, A. (1996), "Characterizing rock masses by the RMI for use in practical rock engineering: Part 1: The development of the Rock Mass index (RMI)", *Tunn. Undergr. Space Technol.*, **11**(2), 175-188.
- Potyondy, D.O. and Cundall, P.A. (2004), "A bonded-particle model for rock", *Int. J. Rock Mech. Min. Sci.*, **41**(8), 1329-1364.
- Senent, S., Mollon, G. and Jimenez, R. (2013), "Tunnel face stability in heavily fractured rock masses that follow the Hoek–Brown failure criterion", *Int. J. Rock Mech. Min. Sci.*, **60**, 440-451.
- Shen, J., Karakus, M. and Xu, C. (2013), "Chart-based slope stability assessment using the Generalized Hoek–Brown criterion", *Int. J. Rock Mech. Min. Sci.*, **64**, 210-219.
- Song, J.B. and Yu, Z.Y. (2001), "Hoek-Brown Strength Criterion and Method Determining Parameters Mands", *J. Southwest Inst. Technol.*, **16**(1), 26-29. [In Chinese]
- Vallejo, L.E. (2012), "Fractal evaluation of the level of alligator cracking in pavements", *Geomech. Eng., Int. J.*, **4**(3), 219-227.
- Wang, Z.J., Ruiken, A., Jacobs, J. and Ziegler, M. (2014), "A new suggestion for determining 2D porosities in DEM studies", *Geomech. Eng.*, **7**(6), 665-678.
- Yang, X.L. and Pan, Q.J. (2015), "Three dimensional seismic and static stability of rock slopes", *Geomech. Eng.*, **8**(1), 97-111.
- Yang, X.L. and Qin, C.B. (2014), "Limit analysis of rectangular cavity subjected to seepage forces based on Hoek–Brown failure criterion", *Geomech. Eng., Int. J.*, **6**(5), 503-515.
- Yang, X.Q., Zhang, L.J. and Ji, X.M. (2013), "Strength characteristics of transversely isotropic rock materials", *Geomech. Eng., Int. J.*, **5**(1), 71-86.
- Yuan, R.F. and Li, Y.H. (2009), "Fractal analysis on the spatial distribution of acoustic emission in the failure process of rock specimens", *Int. J. Min. Met. Mater.*, **16**(1), 19-24.
- Zhang, J.H., He, J.D. and Fan, J.W. (2000), "Rock Mechanical Parameter Study of Xiaowan Project", *Yunnan Water Power*, **16**(2), 26-27. [In Chinese]